INTERNATIONAL JOURNAL OF ROBUST AND NONLINEAR CONTROL
Int. J. Robust Nonlinear Control 2017; **27**:2937–2960
Published online 23 November 2016 in Wiley Online Library (wileyonlinelibrary.com). DOI: 10.1002/rnc.3718

Coordinate frame free Dubins vehicle circumnavigation using only range-based measurements

Dejan Milutinović[1,*,†], David Casbeer[2], Yongcan Cao[3] and Derek Kingston[2]

[1]*University of California, Santa Cruz, CA, USA*
[2]*Control Science Center of Excellence, AFRL, OH, USA*
[3]*University of Texas, at San Antonio, TX, USA*

SUMMARY

The paper presents a feedback control design that allows a Dubins vehicle to enter a circular trajectory using only range-based measurements from the vehicle to the center of the trajectory. The controller is derived and analyzed based on a novel state space kinematic model, with the state that is composed of two continuous and one discrete state variables.The evolution of the discrete state variable is not completely defined by the model and the control design has to deal with the ambiguity of this value. Based on the conditions that need to be satisfied for the controller to work, the closed loop dynamics analysis can be performed based on 2D phase portraits, and it can be shown that the controller can work in the case of the bounded turning rate of the vehicle. The conditions define only bounds for the controller parameters and not their specific values. Therefore, the parameters can be selected based on the maximal working range of the controller and linear quadratic regulator design. The proposed control design is illustrated by 2D phase portraits and simulations describing the control implementation, which is based only on range measurements. Copyright © 2016 John Wiley & Sons, Ltd.

Received 10 April 2016; Revised 30 October 2016; Accepted 31 October 2016

KEY WORDS: Dubins vehicle; feedback linearization; discrete state value ambiguity; phase portrait analysis

1. INTRODUCTION

This paper is motivated by a recent interest in developing control strategies that provide an increased level of the autonomy of small unmanned aerial vehicles (UAVs). In the context of this paper, it means minimizing the amount of information needed for navigation, be it measured on board or provided externally, and therefore reducing communication and vehicle loads. Also, with the increased use of UAVs in civil and commercial applications [1], unsafe operations caused by GPS jamming [2] or GPS spoofing [3] become increasingly relevant. In these situations, only range measurements may be available [4] and a range-only navigation strategy would be required.

For single UAVs, the majority of existing work has been on the development of path planning algorithms for two objectives: (i) the shortest path from one place to another and (ii) the shortest path visiting a set of targets. For instance, a path planning algorithm was proposed in [5] to provide a flyable and safe path for a UAV to move from one place to another while meeting physical constraints, such as minimum accumulative exposure to radar sites and maximum turning rate. In [6], a path planning algorithm was developed to find the minimum-time path from an initial configuration to a final configuration considering a bounded turning rate and the existence of a constant wind. The minimum expected time navigation in reaching a point in the presence of stochastic wind has been

*Correspondence to: Dejan Milutinović, Associate Professor, Computer Engineering Department, University of California, Santa Cruz, CA, USA.
†E-mail: dmilutin@ucsc.edu

considered in [7] and minimum expected path planning through a sequence of points in the presence of stochastic wind was presented in [8]. An evolution-based path generation algorithm for UAVs to conduct oceanic search missions that takes into account realistic weather information was proposed in [9]. A path planning algorithm for a single fixed-wing UAV to photograph a set of stationary ground targets in minimum time was developed in [10], and in [11], single UAV path planning algorithms with the objective to visit a set of dynamic targets in the shortest distance with and without obstacles were developed. One common feature in the aforementioned references is that positioning data obtained from GPS is used in the algorithm development, or it is based on range and bearing measurements.

One typical application for UAVs is the surveillance mission, where the UAV is tasked to orbit around a stationary target at the desired distance [12, 13]. This type of motion is called *circumnavigation* [14]. When GPS is available, a control solution for UAV circumnavigation was given in [15] and can be considered as a path following problem [16–18]. Under the assumption that range and bearing measurements are available, a stochastic optimal control for solving the circumnavigation problem including the case of a sporadic loss of measurements was presented in [19]. When GPS or range and bearing measurements are unavailable, some alternative control solutions were developed to deal with this issue. The circumnavigation of an autonomous agent modeled by a single integrator kinematic model using bearing only measurements was proposed in [13]. Their control is based on an approach in which identification and control problems are solved simultaneously. A similar approach was proposed in [14] for circumnavigation based on range measurements, but again under the assumption of a linear, single integrator kinematic model. A unicycle kinematic model for the UAV has been used in a feedback control based on range and range rate measurements in [20]. The controller is in the form of a stabilizing switching controller that switches between two modes, while the UAV reaches and maintains a desired circular trajectory. Because the unicycle model does not describe the limited UAV's turning rate, the turning rate limit has not been considered in the control design, but it has been addressed through a non-smooth version of the controller. The same unicycle model and a similar control approach have been used in [21], while the limited turning rate was again not a part of the design but was addressed through numerical simulations.

A planar, non-holonomic Dubins vehicle [22] gives a good approximation for trajectories of small, fixed-wing UAV at a constant altitude [23]. The approximation is reasonable if the UAV is accompanied with an autopilot to fly at a fixed altitude with a limited turning rate resulting in a limited roll angle. The sliding mode controls for target following based on range-only measurements have been considered in [24, 25], and the authors included a case of a stationary target. The work in [24] considered the Dubins vehicle navigation that keeps the target in a proximity of the vehicle and navigates it along a trajectory that resembles a curve called an equiangular spiral. This problem is very different from the one considered here, which is to navigate the Dubins vehicle to orbit around a target at a desired distance. On the other hand, the controller [25] is based on an assumption that prevents its use if the vehicle starts too close to the target. Contrary to the controllers in [24, 25], the control design for the Dubins vehicle presented here does not result in any control chattering. More importantly, if the vehicle starts close to the target, our control design guarantees that the vehicle is navigated to the orbit at a desired distance from the target.

The presented feedback control is based on the Dubins vehicle model in a transformed state space, which is derived from a state space transformation. While it is known that the state space transformation of non-holonomic vehicles plays an important role in proving controller stabilities [26, 27], the one presented in this paper is novel to the best of our knowledge, because it transforms the original control problem with three continuous variables into a problem with two continuous and one discrete state variables.

The transformation provides a feedback linearization [28] and control law based on range and range rate measurements, which yields a non-switching control around the steady state. After the transformation, we analyze the dynamical system in the state space, with variables that are not related to any specific coordinate reference frame; therefore, we call the controller *coordinate frame free*. The analysis upon which the controller is based defines conditions that limit the vehicle's turning rate and allows for only one turn before it spirals down to a desired circular orbit. A preliminary version of this work was presented in [29] in which the results for the limited turning rate control

DOI: 10.1002/rnc

were based on graphical arguments without an analytical proof. Here, we provide all results analytically and show that the controller works up to a maximum distance between the orbit center and the vehicle's initial position. Furthermore, we derive conditions describing this maximum distance and use them to select the controller's working range in combination with an optimal control parameter selection approach, for example, the linear quadratic regulator (LQR) design. Finally, a comparison between controllers with a nonoptimal and optimal selection of parameters is provided. The controllers are implemented in discrete time as range measurement only controllers.

In Section 2, we provide the problem formulation, followed by the state transformation and the problem re-formulation in Section 3. The preliminary analysis of the problem is presented in Section 4 and the analysis that deals with the ambiguity of the discrete state, bounded turning rate and stability of the feedback control loop in Section 5. Section 6 gives an example of control parameter selection followed by simulation examples in Section 7 and conclusions in Section 8.

2. PROBLEM FORMULATION

The Dubins vehicle kinematics model is given by

$$\dot{x} = v\cos(\theta(t)) \tag{1}$$

$$\dot{y} = v\sin(\theta(t)) \tag{2}$$

$$\dot{\theta} = \omega(t) \tag{3}$$

where x and y are the coordinates of the vehicle position, $v > 0$ is the constant velocity, θ is the heading angle and ω is the turning rate, which is the only control variable. The model (1)–(3) variables are depicted in Figure 1.

We assume that the center O of the orbit is stationary. The objective is to design a controller providing that the Dubins vehicle circumnavigates around the orbit center O at some desired distance d using range r and range rate measurements $\dot{r}$ only, while the center O position is unknown. We formulate the problem under the assumption that the vehicle has a bounded turning rate

$$A1: \quad -\omega_{max} < \omega < \omega_{max}, \ \ \omega_{max} = \frac{v}{d_{min}} \tag{4}$$

corresponding to the minimal radius $d_{min} > 0$. The second assumption is that for our feedback control $\omega(r, \dot{r})$, there exists a certain minimal distance $R_{max} - 2d_{min} > d > 0$ at which the control saturates for any $\dot{r} \geqslant 0$, that is,

$$A2: \quad (r + 2d_{min} \geqslant R_{max} \text{ and } \dot{r} \geqslant 0) \Rightarrow |\omega(r, \dot{r})| = \omega_{max} \tag{5}$$

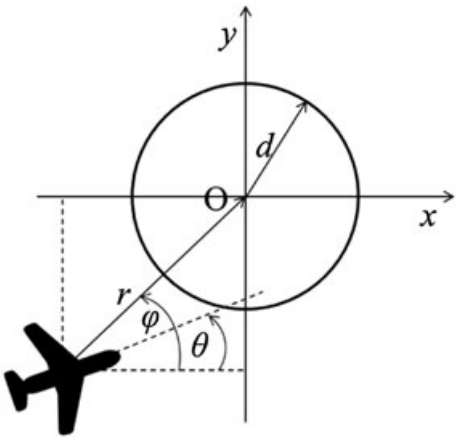

Figure 1. The Dubins vehicle model variable definitions.

DOI: 10.1002/rnc

While the first assumption is realistic, the second assumption is the one to be confirmed by the conditions of Lemma 8. The same lemma also shows that if the initial distance $r(0)$ is smaller than $R_{max} - 2d_{min}$, then under the control proposed in Section 6, the distance $r(t)$ is within the range R_{max} for all t. Formally, we can write it as

$$A2': \quad r(0) + 2d_{min} \geqslant R_{max} \Rightarrow r(t) < R_{max}, \forall t > 0 \tag{6}$$

and this will be used as the assumption until we show in Lemma 8 that it is a corollary of the lemma's conditions and assumption (5).

3. STATE SPACE REFORMULATION

Here, we show that the original problem, defined in x, y, θ state space, can be formulated based on a state space model with three variables, of which one can take only discrete values. The state variables are the distance, r, from the Dubins vehicle to the center and its derivative $\dot{r}$ (Figure 1). The discrete variable $f \in \{-1, 1\}$ relates to the direction of the vehicle circumnavigation around the center O and will be defined below. After we introduce the new state space, we re-formulate the original problem in the new state space.

The distance r from the center O and its derivative are

$$r^2 = x^2 + y^2 \Rightarrow \dot{r} = \frac{x\dot{x} + y\dot{y}}{r}, r \neq 0 \tag{7}$$

We can define the angle φ as (Figure 1)

$$x = -r\cos\varphi, \quad y = -r\sin\varphi \tag{8}$$

and find that $\dot{r} = -\cos\varphi \cdot v\cos\theta - \sin\varphi \cdot v\sin\theta$, that is,

$$\dot{r} = -v\cos(\varphi - \theta), r \neq 0 \tag{9}$$

that also states that $|\dot{r}| \leqslant v$. Taking the derivative of $\dot{r}$ and after the substitution $\dot{\theta} = \omega$, we obtain

$$\ddot{r} = v\sin(\varphi - \theta)(\dot{\varphi} - \omega), r \neq 0 \tag{10}$$

From $\varphi = \arctan\frac{-y}{-x}$, we can derive that

$$\dot{\varphi} = \frac{x\dot{y} - y\dot{x}}{x^2 + y^2} = \frac{-r\cos\varphi \cdot v\sin\theta + r\sin\varphi \cdot v\cos\theta}{r^2}, r \neq 0 \tag{11}$$

and conclude that

$$\dot{\varphi} = \frac{v}{r}\sin(\varphi - \theta), r \neq 0 \tag{12}$$

To express φ as a function of r and $\dot{r}$, we use (9) to conclude

$$\cos^2(\varphi - \theta) = \left(\frac{\dot{r}}{v}\right)^2 \Rightarrow \sin(\varphi - \theta) = f\sqrt{1 - \left(\frac{\dot{r}}{v}\right)^2}, r \neq 0 \tag{13}$$

where f can only take the values -1 and 1, that is, $f \in \{-1, 1\}$ is the discrete variable; consequently,

$$\dot{\varphi} = f\frac{1}{r}\sqrt{v^2 - \dot{r}^2}, r \neq 0 \tag{14}$$

and after the substitution of (13) and (14) in (10), we finally obtain

$$\ddot{r} = \frac{1}{r}\left(v^2 - \dot{r}^2\right) - f\omega\sqrt{v^2 - \dot{r}^2}, r \neq 0 \tag{15}$$

Let us define the first state as $x_1 = r$ and the second as $x_2 = \dot{r}$; therefore, it also satisfies $|x_2| \leqslant v$. Then, the state space model for $x_1 > 0$ and $x_2 \in [-v, v]$ is

$$\dot{x}_1 = x_2, \tag{16}$$

DOI: 10.1002/rnc

$$\dot{x}_2 = \frac{1}{x_1}\left(v^2 - x_2^2\right) - f(t)\omega\sqrt{v^2 - x_2^2} \tag{17}$$

in which we use the discrete state variable $f(t)$ and the notation emphasizing that its value can change in time. Keeping in mind that $x_1 = r > 0$ and $x_2 = \dot{r}$, the meaning of the discrete variable $f(t) \in \{-1, 1\}$ can be understood from a comparison between (12) and (14)

$$\dot{\varphi} = \frac{v}{r}\sin(\varphi - \theta) = \frac{v}{x_1} f(t)\sqrt{1 - \left(\frac{x_2}{v}\right)^2} \tag{18}$$

If the vehicle's heading angle and relative position to the center O are such that φ increases ($\dot{\varphi} > 0$), then $f(t) = +1$. Otherwise, if φ decreases ($\dot{\varphi} < 0$), then $f(t) = -1$. The sign of $f(t)$ depends on $\varphi - \theta$, and it can switch when $\varphi - \theta = \pi$, or $\varphi - \theta = 0$. These correspond to the state space points when the vehicle is heading to the center O ($x_2 = -v$) or in the opposite direction of it ($x_2 = v$), respectively. At these specific points, the value of $f(t)$ is ambiguous. In addition to it, for $x_1(t) = 0$, the value of $x_2(t)$ is ambiguous. Our control based on models (16) and (17) has to deal with all these ambiguities, as well as the fact that the model does not define the evolution of $f(t)$.

With models (16) and (17), the circumnavigation goal, which is that the vehicle orbits around the point O at a desired distance d, becomes that the state variables x_1 and x_2 have to converge to $x_1 = d$ and $x_2 = 0$. At that point, all model variables x_1, x_2, and f are well defined. Because $v \geqslant x_2 = \dot{r}$, we have $\frac{1}{x_1}(v^2 - x_2^2) \geqslant 0$, which implies that the state space equations (16) and (17) can have the fixed point $x_1 = d, x_2 = 0$, that is, the vehicle can circulate ($\omega \neq 0$) around the center O at the fixed distance d only if $f(t)\omega > 0$. In other words, if at the fixed point the vehicle has the counter-clockwise rotation ($\omega > 0$), then $f(t) = 1$. Otherwise, if at the fixed point the vehicle has the clockwise rotation ($\omega < 0$), then $f(t) = -1$.

In summary, based on the model presented in this section, the control problem from the previous section is described by the following *problem formulation:* find a control ω so that for the state space models (16) and (17) and the assumptions A1 (4) and A2 (6), the state $(x_1(t), x_2(t))$, $x_1 \in [0, R_{max} - 2d_{min}]$, $x_2 \in [-v, v]$ converges to the point $(d, 0)$.

4. PRELIMINARY ANALYSIS OF FEEDBACK CONTROL

In this section, we present a feedback control that inspired our main result. It is based on the assumption that the states $x_1(t)$ and $x_2(t)$ are measured, while $f(t)$ is a known value that does not change in time, that is, $f(t) = f(0)$, and $f(0)$ is a known value of $f(t)$ at $t = 0$. Here, we allow for the unbounded control ω and in models (16) and (17), the control cancels terms in (17) that are unbounded as $x_1 \to 0$. These are the reasons why the analysis is preliminary; however, we use it to define the form of the feedback control in our main result presented in the next section.

Once we present Lemma 1 with regard to the preliminary results of the unbounded feedback control law, in Lemma 2, we analyze special initial conditions in which the preliminary feedback control from Lemma 1 is either undefined or is unbounded. For these initial conditions, we analyze the effect of the maximum turning rate control $\omega = \hat{f}\omega_{max}$, $\hat{f} \in \{-1, 1\}$ to show the effect of the control on $f(t)$ and state variable x_2 after a small time $\tau > 0$ following the initial time point. The Lemma 2 results are used in Lemma 5 of the next section. Lemmas 1 and 2 and their proofs are provided in the succeeding text.

Lemma 1

Under the assumptions that $|x_2(t)| < v$ for all $t \geqslant 0$ and that on the same time interval $f(t) = f(0) \in \{-1, 1\}$ is known, then the point $(d, 0)$ is asymptotically stable under control

$$\omega = \hat{f}u, \quad \hat{f} = f(0) \tag{19}$$

$$u(x_1, x_2) = \frac{1}{\sqrt{v^2 - x_2^2}}\left(\frac{c_1(x_1 - d)}{c_2} + \frac{(v^2 - x_2^2)}{x_1} + c_3 x_2\right) \tag{20}$$

DOI: 10.1002/rnc

Proof
Let us define a Lyapunov function

$$V(x_1, x_2, \hat{f}) = \frac{c_1}{2}(x_1 - d)^2 + \frac{c_2}{2}x_2^2 \tag{21}$$

with the derivative

$$\dot{V} = c_1(x_1 - d)x_2 + c_2 x_2 \left[\frac{1}{x_1}(v^2 - x_2^2) - f(t)\omega\sqrt{v^2 - x_2^2}\right]$$

If we substitute ω from (19), where $\hat{f} = f(0)$, $f(t) = f(0)$, we have that $f(t)^2 = 1$ and

$$\dot{V} = x_2 \left[c_1(x_1 - d) + \frac{c_2}{x_1}(v^2 - x_2^2) - c_2 u\sqrt{v^2 - x_2^2}\right]$$

and after the substitution of (20) in the given expression, we obtain

$$\dot{V} = -c_2 c_3 x_2^2 \leqslant 0 \tag{22}$$

A set of points where $\dot{V} = 0$ is $S_{\dot{V}=0} = \{(x_1, x_2) | x_2 = 0\}$. According to LaSalle's theorem [30], when $t \to \infty$, the system approaches the largest invariant set inside $S_{\dot{V}=0}$. When controls (19) and (20) are substituted in (16) and (17), we obtain

$$\dot{x}_1 = x_2 \tag{23}$$

$$\dot{x}_2 = -\frac{c_1(x_1 - d)}{c_2} - c_3 x_2 \tag{24}$$

describing $\dot{x}_1$ and $\dot{x}_2$, respectively. For all points of $S_{\dot{V}=0}$, we have $\dot{x}_1 = 0$ and $\dot{x}_2 \neq 0$ except for the point $x_1 = d$, $x_2 = 0$, where $\dot{x}_1 = 0$ and $\dot{x}_2 = 0$ (expressions (23) and (24)). The point $(d, 0)$ is the only fixed point, and the largest invariant set inside $S_{\dot{V}=0}$ is the point $(d, 0)$. □

Lemma 2 (Special initial conditions)
Let us assume that $f(0) \in \{-1, 1\}$ is known and the initial condition satisfies $x_1(0) = 0$, or $x_1(0) > 0$ and $|x_2(0)| = v$. If we choose $\hat{f} = 1$ (or $\hat{f} = -1$), then under the control

$$\omega = \hat{f}\omega_{max} \tag{25}$$

there exists a small time $\tau > 0$ such that $x_1(\tau) > 0$, $|x_2(\tau)| < v$ and $f(\tau) = \hat{f}$.

Proof
We start our proof with the reminder that $x_2 = \dot{r}$, $\omega = \dot{\theta}$ and that $x_2(t)$ is bounded, that is, $-v \leqslant x_2(t) \leqslant v$. Part 1 of the proof deals with the case $x_1(0) > 0$, $x_2 = v$, Part 2 with $x_1(0) > 0$, $x_2 = -v$, and Part 3 of the proof with $x_1(0) = 0$.

(*Part 1a*) For $x_1(0) > 0$, $x_2(0) = v$, the relative bearing angle, which is the difference between φ and θ (Figure 1) at $t = 0$, is $\varphi(0) - \theta(0) = \pi$ (expression (9)) and $\dot{\varphi}(0) = 0$ (expression (12)). Therefore, $\omega = \omega_{max} = v/d_{min}$ or $\omega = -\omega_{max} = -v/d_{min}$ for a small $\tau > 0$ yields

$$\varphi(\tau) - \theta(\tau) = \varphi(0) + \dot{\varphi}(0)\tau - \theta(0) - \omega\tau + o(\tau) = \pi - \omega\tau + o(\tau) \neq \pi \tag{26}$$

and, consequently, from (9), it follows that $x_2(\tau) < v$, that is, $|x_2(\tau)| < v$.

(*Part 1b*) If we set $\hat{f} = 1$, from (25), we can conclude that $\omega > 0$, $\dot{\varphi}(0) = 0$ and from (26) that $\varphi(\tau) - \theta(\tau) < \pi$. From the latter and expression (18), we can conclude that $f(\tau) = 1$, that is, $f(\tau) = \hat{f}$. If we set $\hat{f} = -1$, then from (25), it follows that $\omega < 0$, $\dot{\varphi}(0) = 0$ and from (26) that $\varphi(\tau) - \theta(\tau) > \pi$. Therefore, $f(\tau) = -1$, and $f(\tau) = \hat{f}$ is obtained again.

DOI: 10.1002/rnc

(*Part 2a*) For $x_1(0) > 0$, $x_2(0) = -v$, the relative bearing angle at $t = 0$ is $\varphi(0) - \theta(0) = 0$ (expression (9)) and $\dot{\varphi}(0) = 0$ (expression (12)). Therefore, $\omega = \omega_{max}$ or $\omega = -\omega_{max}$ yields

$$\varphi(\tau) - \theta(\tau) = \varphi(0) + \dot{\varphi}(0)\tau - \theta(0) - \omega\tau + o(\tau) = -\omega\tau + o(\tau) \neq 0 \tag{27}$$

and again, from (9), it follows that $x_2(\tau) > -v$, , that is, $|x_2(\tau)| < v$. With this and the conclusion of Part 1*a* of the proof, we prove that from $|x_2(0)| = v$ and $\omega = \omega_{max}$ or $\omega = -\omega_{max}$ follows that $|x_2(\tau)| < v$.

(*Part 2b*) If we set $\hat{f} = 1$, from (25), we can conclude that $\omega < 0$, $\dot{\varphi}(0) = 0$ and from (27) that $\varphi(\tau) - \theta(\tau) > 0$. From the latter and expression (18), we can conclude that $f(\tau) = 1$, that is, $f(\tau) = \hat{f}$. If we set $\hat{f} = -1$, then from (25), it follows that $\omega > 0$, $\dot{\varphi}(0) = 0$ and that $\varphi(\tau) - \theta(\tau) < 0$. Therefore, $f(\tau) = -1$, and once again we conclude that $f(\tau) = \hat{f}$. With this and the conclusion of Part 1*b* of the proof, we prove that from $|x_2(0)| = v$ and $\omega = \hat{f}\omega_{max}$, it always follows that $f(\tau) = \hat{f}$.

(*Part 3*) For the case $x_1(0) = 0$, neither $x_2(0)$ nor $\phi(0)$ is defined. Figure 2 shows the vehicle in such a position, and without losing generality of our analysis, we depict it with the heading angle $\theta = \pi/2$. From Figure 2(*a*), which corresponds to $\hat{f} = 1$, we can find that for an infinitesimally small τ_1 and positive $\omega = \omega_{max} > 0$, $\delta_x = v/\omega_{max}\sin(\omega_{max}\tau_1)$ and $\delta_y = v/\omega_{max}(1 - \cos(\omega_{max}\tau_1))$, and by using $r = \sqrt{\delta_x^2 + \delta_y^2}$, we obtain

$$r = x_1 = 2d_{min}\sin\frac{\omega_{max}\tau_1}{2} = d\omega_{max}\tau_1 + o(\tau_1^3) \tag{28}$$

$$\dot{r} = x_2 = d\omega_{max}\cos\frac{\omega_{max}\tau_1}{2} = d\omega_{max} + o(\tau_1^2) \tag{29}$$

in which $o(\tau_1^3)$ and $o(\tau_1^2)$ denote infinitesimally small values of the $3rd$ and $2nd$ order, respectively, that can be neglected at the scale of infinitesimally small τ_1. This means that after a small $\tau_1 > 0$, $x_1(\tau_1) > 0$ and $x_2(\tau_1) = v$. The same conclusion can be derived if we consider $\hat{f} = -1$ and the corresponding Figure 2(*b*). Now, if we consider τ_1 as the initial time point, we can follow the reasoning from Part 1 of the proof that deals with the initial state $x_1 > 0$, $x_2 = v$ to show that for $\omega = \hat{f}\omega_{max}$, it follows that $f(\tau) = \hat{f}$ and $|x_2(\tau)| < v$. With this and the conclusions of Part 2*a* and Part 2*b*, we finish the proof.

□

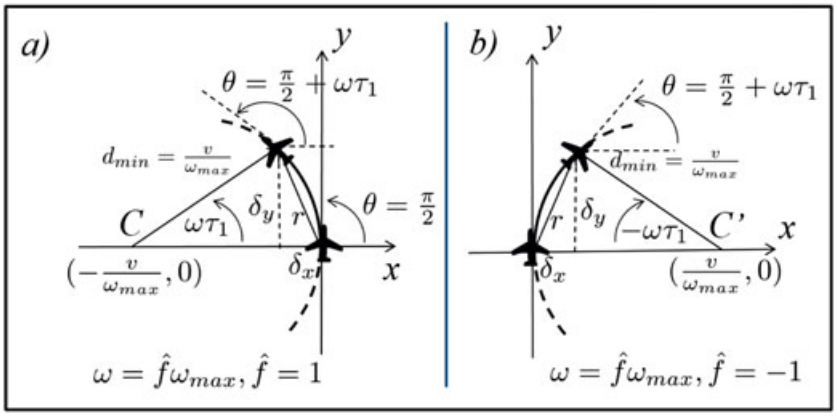

Figure 2. The Dubins vehicle with the initial position at the center O, $x_1 = 0$ and turning with the maximal turning rate $\omega_{max} = v/d_{min}$ for (a) $\hat{f} = 1$ and (b) $\hat{f} = -1$. [Colour figure can be viewed at wileyonlinelibrary.com]

DOI: 10.1002/rnc

5. CONTROL WITH BOUNDED TURNING RATE

The controller that we propose is based on the continuous state variable measurements $x_1 = r$ and $x_2 = \dot{r}$, and we do not assume that the discrete value $f(t) \in \{-1, 1\}$ is known, that is, we deal with the ambiguity of its value. The proposed control is

$$\omega = \hat{f} u \tag{30}$$

with a free choice of the variable $\hat{f} \in \{-1, 1\}$ and u computed based on positive parameters $c_1, c_2, c_3 > 0$ as

$$u = \begin{cases} \omega_{max}, & u_c > \omega_{max} \\ -\omega_{max}, & u_c < -\omega_{max} \\ u_c, & \text{otherwise} \end{cases} \tag{31}$$

and

$$u_c = \begin{cases} \frac{1}{\sqrt{v^2 - x_2^2}} \left(\frac{c_1(x_1 - d)}{c_2} + \frac{(v^2 - x_2^2)}{x_1} + c_3 x_2 \right), & x_1 \neq 0 \\ \omega_{max}, & x_1 = 0 \end{cases} \tag{32}$$

The control has the bounded turning rate because $\omega_{max} = v/d_{min}$, where d_{min} is the vehicle's minimal turning radius, therefore, it satisfies the assumption A1 (4). We use the assumption A2 (5) to define constraints between the control parameters providing that A2' (6) is satisfied, which is the topic of Lemma 6. This lemma justifies the use of A2' (6) as an assumption in proving Lemmas 3–5. These results are used in the theorem at the end of the section to prove that the point $(d, 0)$ is the stable fixed point for systems (16)–(17) under controls (31) and (32).

In Lemma 3, we show that if at a current time t, $\hat{f} \neq f(t)$, then the trajectories of the system will reach a point in which either $x_2 = v$ or $x_2 = -v$. Lemma 4 provides conditions that at points with $x_1 > 0$ and $x_2 = v$ ($x_2 = -v$), the control variable u is positive $u = \omega_{max}$ (is negative $u = -\omega_{max}$). The conditions of Lemmas 3 and 4 are used in the proof of Lemma 5, which states conditions providing the existence of a trapping region for the system trajectories in the x_1, x_2 plane with $\hat{f} = f(t)$. The trapping region is illustrated in Figure 3 together with the single fixed point at $(d, 0)$, and the assumption A2' (6) used in the proofs of Lemmas 3–6 is justified in Lemma 6 based on the conditions that satisfy A2 (5).

The whole set of parameter conditions from the Lemma 3–6 conditions can be summarized with the condition

$$\text{(C1)} \qquad \sqrt{d_{min} \frac{c_1(R_{max} - 2d_{min} - d)}{c_2}} > v > \max\left\{ \frac{c_1(R_{max} - d)}{c_2 c_3}, \frac{c_1 d}{c_2 c_3}, d\sqrt{\frac{c_1}{8c_2}} \right\} \tag{33}$$

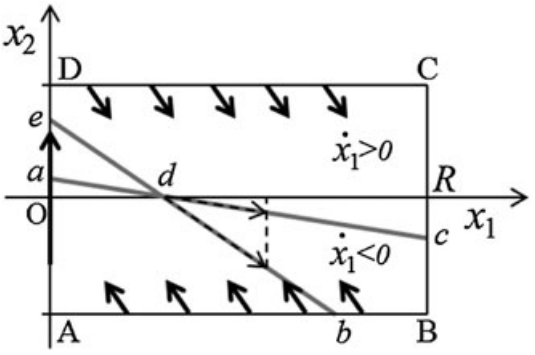

Figure 3. The eigenvectors $[1\ \lambda_1]^T$, $[1\ \lambda_2]^T$ (dashed arrows) and the trapping region A, B, C, D.

DOI: 10.1002/rnc

Theorem 3 introduces two more conditions, the first one providing that the fixed point $(d, 0)$ has two eigenvalues $\lambda_2 < \lambda_1 < 0$

$$\lambda_{1,2} = \frac{-c_3 \pm \sqrt{c_3^2 - 4c_1/c_2}}{2} \tag{34}$$

that are real negative values for

$$\text{(C2)} \qquad c_3 > 2\sqrt{c_1/c_2} \tag{35}$$

and the second providing that the system under control does not have limit cycles in the phase plane x_1-x_2, which is included in the condition below. On the line segment $\overline{dc}$ (Figure 3) that connects the fixed point $(d, 0)$ with the boundary A, B, C, D along the line $x_2 = \lambda_1(x_1 - d)$ defined by the eigenvector $[1\ \lambda_1]^T$, $\lambda_2 < \lambda_1 < 0$, the inequality

$$\text{(C3)} \qquad \left(\frac{c_1(x_1 - d)}{c_2} + \frac{(v^2 - x_2^2)}{x_1} + c_3 x_2\right)^2 < \frac{v^2(v^2 - x_2^2)}{d_{min}^2} \tag{36}$$

has to be satisfied up to R_{max}. After the substitution of x_2, the inequality is

$$\left(\frac{c_1(x_1 - d)}{c_2} + \frac{(v^2 - \lambda_1^2(x_1 - d)^2)}{x_1} + c_3\lambda_1(x_1 - d)\right)^2 < \frac{v^2(v^2 - \lambda_1^2(x_1 - d)^2)}{d_{min}^2} \tag{37}$$

and the x_1 value at which the inequality is invalid for the first time is R_{max} in the conditions C1 and C2.

In the succeeding text, we provide the statements and proofs of lemmas and the theorem from this section.

Lemma 3
If $\hat{f} \neq f(t)$, $|x_2(t_0)| < v$, $R_{max} > d$ and $v > \max\left\{\frac{c_1(R_{max}-d)}{c_2c_3}, \frac{c_1 d}{c_2c_3}, d\sqrt{\frac{c_1}{8c_2}}\right\}$, then under controls (31) and (32), there exists a time point $t_c > 0$ such that $|x_2(t_c)| = v$, or $x_1(t_c) = 0$.

Proof
Let us first notice that for $\hat{f} \neq f(t)$, expression (16) does not change because it depends only on x_2. In other words, for $x_2 > 0$, we have $\dot{x}_1 > 0$ and, for $x_2 < 0$, we have $\dot{x}_1 < 0$.

Based on the lemma conditions, we know from (17) that if u_c is positive and the control not saturated, that is, $0 < u_c < \omega_{max} = v/d_{min}$, then for $x_2 \geqslant 0$, we have

$$\dot{x}_2 = \frac{v^2 - x_2^2}{x_1} + u_c\sqrt{v^2 - x_2^2} > 0 \tag{38}$$

In the saturated control case $u_c > \omega_{max}$, the derivative $\dot{x}_2$ is positive, that is,

$$\dot{x}_2 = \frac{v^2 - x_2^2}{x_1 + \omega_{max}}\sqrt{v^2 - x_2^2} > 0 \tag{39}$$

for all $x_2 \in [0, v)$ because all terms are positive.

If u_c is negative, the control is not saturated $-\omega_{max} < u_c < 0$ and $\hat{f} \neq f(t)$. Then $\hat{f}f(t) = -1$ and we know that under control (20), (16) and (17) result in

$$\dot{x}_1 = x_2 \tag{40}$$

$$\dot{x}_2 = \frac{1}{x_1}(v^2 - x_2^2) + u_c\sqrt{v^2 - x_2^2} \tag{41}$$

$$= \frac{2}{x_1}(v^2 - x_2^2) + \frac{c_1(x_1 - d)}{c_2} + c_3 x_2 \tag{42}$$

DOI: 10.1002/rnc

where $\dot{x}_2$ can be rewritten as

$$\dot{x}_2 = g(x_2) = -\frac{2}{x_1}x_2^2 + c_3 x_2 + \frac{2}{x_1}v^2 + \frac{c_1(x_1 - d)}{c_2} \tag{43}$$

For a fixed x_1, the function $g(x_2)$ is concave and has two zeros $x_2^{\mathrm{II}} \geqslant x_2^{\mathrm{I}}$

$$x_2^{\mathrm{I,\,II}} = \frac{c_3 x_1}{4} \pm \sqrt{\frac{c_3^2 x_1^2}{16} + v^2 + \frac{c_1}{2c_2}x_1(x_1 - d)} \tag{44}$$

From $x_2^{\mathrm{II}} > v$, the condition $\frac{c_1}{c_2}(x_1 - d) > -vc_3$ follows. Because $c_1/c_2 > 0$, $d > 0$ and $x_1 \geqslant 0$, the lower bound on the left side of the condition inequality is $-\frac{c_1}{c_2}d$. Therefore, $x_2^{\mathrm{II}} > v$ holds true regardless of the x_1 value if $-\frac{c_1}{c_2}d > -vc_3$. Because $c_3 > 0$, the last inequality can be written as

$$v > \frac{c_1 d}{c_2 c_3} \tag{45}$$

that is the condition that guarantees that $x_2^{\mathrm{II}} > v$ regardless of the x_1 value. Moreover, $x_2^{\mathrm{I}} \geqslant 0$ is possible only if there is x_1 such that

$$v^2 + \frac{c_1}{2c_2}x_1(x_1 - d) \leqslant 0 \tag{46}$$

To assure that this is not possible, that is, that the expression on the left side of the inequality is always positive, we find its zeros

$$x_1^{\mathrm{I,II}} = \frac{d}{2} \pm \sqrt{\frac{d^2}{4} - 2\frac{c_2}{c_1}v^2} \tag{47}$$

from which it follows that the zeros are conjugate complex under the condition

$$\frac{c_1 d^2}{8c_2} < v^2 \tag{48}$$

Similarly, $x_2^{\mathrm{I}} \leqslant -v$ only if there is x_1 such that

$$\frac{c_1}{c_2 c_3}(x_1 - d) \geqslant v \tag{49}$$

which is impossible if

$$\frac{c_1}{c_2 c_3}(R_{max} - d) < v \tag{50}$$

In summary, $x_2^{\mathrm{I}} \geqslant 0$ and $x_2^{\mathrm{I}} \leqslant -v$ are impossible if the (48) and (50) conditions are satisfied, respectively. This means that $-v < x_2^{\mathrm{I}} < 0$ and $x_2^{\mathrm{II}} > v$, and from this, it follows that for $0 \leqslant x_2 \leqslant v$, the time derivative is strictly positive, $\dot{x}_2 > 0$ and for $x_2 = -v$, $\dot{x}_2 < 0$.

If u_c is negatively saturated, that is, $u_c < u = -\omega_{max} < 0$ and $\hat{f} \neq f(t)$, then $\hat{f}\,f(t) = -1$ and from that it follows

$$\dot{x}_2 = \frac{v^2 - x_2^2}{x_1} - \omega_{max}\sqrt{v^2 - x_2^2} > 0 \tag{51}$$

because, in this case, the value of $-\omega_{max}$ is less negative than the corresponding value $u_c < -\omega_{max}$ in (41).

DOI: 10.1002/rnc

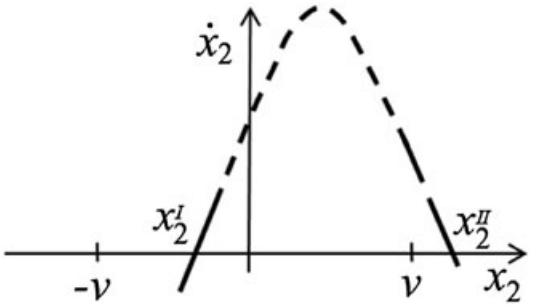

Figure 4. Sketch of $\dot{x}_2 = g(x_2)$ for $\hat{f} \neq f(t)$ and $v > \max\left\{\frac{c_1(R_{max}-d)}{c_2c_3}, \frac{c_1 d}{c_2c_3}, d\sqrt{\frac{c_1}{8c_2}}\right\}$.

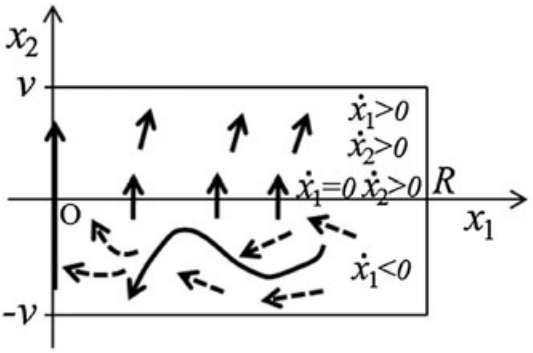

Figure 5. Sketch of the phase portrait for $\hat{f} \neq f(t)$ and $v > \max\left\{\frac{c_1(R_{max}-d)}{c_2c_3}, \frac{c_1 d}{c_2c_3}, d\sqrt{\frac{c_1}{8c_2}}\right\}$.

Now, for $x_2 < 0$, the derivative $\dot{x}_2$ can be 0, but because of (16), for all points $x_2 < 0$, we have $\dot{x}_1 < 0$ and no fixed point can exist.

Finally, we can sketch a phase portrait for the system (Figure 5). In all points where $v > x_2 > 0$, we have $\dot{x}_1 > 0$ and $\dot{x}_2 > 0$. Moreover, for $x_2 = 0$ and $x_1 > 0$, we have $\dot{x}_1 = 0$ and $\dot{x}_2 > 0$. This means that any system trajectory that starts in the region $0 > x_2 > -v$, where $\dot{x}_1 < 0$, will end up either on the line $x_2 = v$, or $x_2 = -v$, or $x_1 = 0$. □

Remark 1

For an illustration of the proof, the function $g(x_2)$ from (43), under conditions (48) and (50), is sketched in Figure 4. This figure shows that if $v \geqslant x_2 \geqslant 0$, then $\dot{x}_2 > 0$. Now, we can sketch the phase portrait for (40) and (41), which is depicted in Figure 5. In all points where $v \geqslant x_2 > 0$, we have $\dot{x}_1 > 0$ and $\dot{x}_2 > 0$. For $x_2 = 0$ and $x_1 > 0$, we have $\dot{x}_1 = 0$ and $\dot{x}_2 > 0$, and for $x_2 < 0$, we have $\dot{x}_1 = x_2 < 0$. Any system trajectory that starts in the region $v > x_2 > -v$ ends up either on the line $x_2 = v$, or $x_2 = -v$, or $x_1 = 0$.

Remark 2

The case $x_1(t_c) = 0$ is the special one in which the vehicle goes directly through the center O. Therefore, the velocity just before hitting the center is $x_2(t_c^-) = -v$ and just after leaving the center the value is $x_2(t_c^+) = v$. This transition is depicted with the arrow for $x_1 = 0$. Therefore, we can even conclude that in all cases, the system trajectories reach a point with $|x_2| = v$.

Lemma 4

If $v > \max\left\{\frac{c_1(R_{max}-d)}{c_2c_3}, \frac{dc_1}{c_2c_3}\right\}$, then at the points where, $x_1 > 0$ and $x_2 = v$ ($x_2 = -v$), the control u is positive $u = \omega_{max}$ (negative $u = -\omega_{max}$).

DOI: 10.1002/rnc

Proof
To find the control value at the point $x_2 = v$, we consider the limit of control u when $x_2 \to v^-$. We can find it by rewriting (32) as

$$u_c = \left(\frac{c_1(x_1 - d)}{c_2\sqrt{v^2 - x_2^2}} + \frac{\sqrt{v^2 - x_2^2}}{x_1} + \frac{c_3 x_2}{\sqrt{v^2 - x_2^2}} \right) \tag{52}$$

from which can be concluded that because of the saturation (31) in the limit of $x_2 \to v^-$, we have

$$u = sgn\left[\frac{c_1(x_1 - d)}{c_2} + c_3 v \right] \omega_{max} \tag{53}$$

Therefore, at $x_2 = v$, the control variable u is positive if

$$\frac{c_1(x_1 - d)}{c_2} + c_3 v > 0 \tag{54}$$

which results in

$$x_1 > -c_3 c_2 / c_1 v + d \tag{55}$$

Because $x_1 > 0$, we can substitute it in the given expression to obtain $0 > -c_3 c_2 / c_1 v + d$, which yields the condition

$$v > \frac{d c_1}{c_2 c_3} \tag{56}$$

Now, we consider the limit of the control variable u when $x_2 \to -v^+$ and use (52), as well as saturation (31) to find that at $x_2 = -v$, we have

$$u = sgn\left[\frac{c_1(x_1 - d)}{c_2} - c_3 v \right] \omega_{max} \tag{57}$$

that is negative for

$$\frac{c_1(x_1 - d)}{c_2} - c_3 v < 0 \tag{58}$$

and because $x_1 < R_{max}$, it results in the condition

$$\frac{c_1(R_{max} - d)}{c_2 c_3} < v \tag{59}$$

Both conditions, (56) for $x_2 = v \Rightarrow u = \omega_{max}$ and (59) for $x_2 = -v \Rightarrow u = \omega_{max}$, can be described by a single expression

$$v > \max\left\{ \frac{c_1(R_{max} - d)}{c_2 c_3}, \frac{d c_1}{c_2 c_3} \right\} \tag{60}$$

which finalizes the proof. □

Lemma 5
Let us assume that the assumption A2' (6) and condition $v > \max\left\{ \frac{c_1(R_{max}-d)}{c_2 c_3}, \frac{c_1 d}{c_2 c_3}, d\sqrt{\frac{c_1}{8c_2}} \right\}$ are satisfied. Then all the system trajectories are after a sufficiently long time (including zero if with $\hat{f} = f(0)$) trapped in the region of the x_1, x_2 plane bounded by the segments $x_1 = 0$, $x_2 = v$, $x_1 = R_{max}$, and $x_2 = -v$ with $\hat{f} = f(t)$.

DOI: 10.1002/rnc

Remark 3
Because of the assumption A2' (6), we know that $0 \leqslant x_1(t) \leqslant R_{max}$ and that $-v \leqslant x_2(t) \leqslant v$, and by this lemma, we prove that all trajectories end up with $f(t) = \hat{f}$, which is the only way we can claim that the trapping region exists. Otherwise, the system trajectories would be able to jump back and forth between trajectories with $\hat{f} = f(t)$ and $\hat{f} \neq f(t)$.

Proof

Following Lemma 3, we can state that at some time point t_c, the system trajectories reach either a point with $|x_2(t_c)| = v$, or a point with $x_1(t_c) = 0$. Therefore, we divide the proof into three parts. Part *a* analyzes the case $\hat{f} \neq f(t)$, $x_1(t_c) > 0$, Part *b* analyzes the case $\hat{f} = f(t)$, $x_1(t_c) > 0$, and Part *c* deals with $x_1(t_c) = 0$, as well a situation when $x_1(0) = 0$ or $|x_2(0)| = v$ □

Part a: For $\hat{f} \neq f(t)$, let us consider the case $x_1(t_c) > 0$, $x_2(t_c) = v$. At the time point t_c, following Lemma 4, we know that the value $u(t_c) = \omega_{max}$, which is based on $\lim_{x_2 \to v^-} u = \omega_{max}$, while the limit is not dependent on $f(t)$, or $\hat{f}$. At the time t_c^-, just before the time point t_c, we have $\hat{f} \neq f(t_c^-)$ and let us assume that at the time t_c^+, just after the time point t_c, we again have $\hat{f} \neq f(t_c^+)$, that is, $\hat{f} f(t_c^+) = -1$. If this is the case, we have $\lim_{t \to t_c^+} \dot{x}_2(t)$ equal to

$$\lim_{t \to t_c^+} \left\{ \frac{v^2 - x_2(t)^2}{x_1} - \hat{f} f(t) u(t) \sqrt{v^2 - x_2^2} \right\} \tag{61}$$

that is, because of $t \to t_c^+ \Rightarrow x_2 \to v^-$, we can rewrite it as

$$\lim_{x_2 \to v^-} \sqrt{v^2 - x^2} \left\{ \frac{\sqrt{v^2 - x_2(t)^2}}{x_1} + u(t) \right\} \tag{62}$$

and after the substitution $\lim_{x_2 \to v^-} u(t) = \omega_{max}$ and the introduction of $\varepsilon > 0$, to substitute $x_2(t) \to v^-$ with $\varepsilon \to 0^+$, we obtain

$$\lim_{t \to t_c^+} \dot{x}_2(t) = \lim_{\varepsilon \to 0^+} \sqrt{v^2 - (v - \varepsilon)^2} \left\{ \frac{\sqrt{v^2 - (v - \varepsilon)^2}}{x_1} + \omega_{max} \right\} \tag{63}$$

$$= \lim_{\varepsilon \to 0^+} \sqrt{\varepsilon} \sqrt{2v + \varepsilon} \left\{ \frac{\sqrt{\varepsilon} \sqrt{2v + \varepsilon}}{x_1} + \omega_{max} \right\} \tag{64}$$

which means that $\lim_{t \to t_c^+} \dot{x}_2(t) \to 0^+$, that is, that $\dot{x}_2(t_c^+) > 0$, which is impossible because $x_2(t_c) = v$ and $-v \leqslant x_2(t) \leqslant v$. Therefore, by contradiction, $\hat{f} = f(t_c^+)$. We can also check from (61) that in that case

$$\lim_{t \to t_c^+} \dot{x}_2(t) = \lim_{\varepsilon \to 0^+} \sqrt{\varepsilon} \sqrt{2v + \varepsilon} \left\{ \frac{\sqrt{\varepsilon} \sqrt{2v + \varepsilon}}{x_1} - \omega_{max} \right\} \tag{65}$$

and that $\dot{x}_2(t_c^+) < 0$.

Repeating the similar analysis for $\hat{f} \neq f(t)$, but for $x_2(t_c) = -v$ and $\lim_{t \to t_c^+} \dot{x}_2(t)$ and $t \to t_c^+ \Rightarrow x_2 \to -v^+$ results in

$$\lim_{t \to t_c^+} \dot{x}_2(t) = \lim_{\varepsilon \to 0^+} \sqrt{\varepsilon} \sqrt{2v - \varepsilon} \left\{ \frac{\sqrt{\varepsilon} \sqrt{2v - \varepsilon}}{x_1} - \omega_{max} \right\} \tag{66}$$

which means that $\lim_{t \to t_c^+} \dot{x}_2(t) \to 0^-$, that is, that $\dot{x}_2(t_c^+) < 0$, which is impossible because $x_2(t_c) = -v$ and $-v \leqslant x_2(t) \leqslant v$. Therefore, by contradiction, $\hat{f} = f(t_c^+)$ and because of that $\dot{x}_2(t_c^+) > 0$.

DOI: 10.1002/rnc

Part b: In the case that $\hat{f} = f(t)$, we should show that if a system trajectory reaches the point $x_2(t_c) = v$ (or a point with $x_2 = -v$) at a time point t_c, then the sign of $f(t)$ does not change. To prove that, we are going to use contradiction arguments similar to those used in Part *a* of the proof.

Let us assume that the sign of $f(t)$ can change. If that happens, then just before the time point t_c, we have $\hat{f} = f(t_c^-)$ and just after the time point t_c, we have $\hat{f} \neq f(t_c^+)$, that is, $\hat{f} f(t_c^+) = -1$. In this case, $x_2 \to v^-$ consider the limit $\lim_{t \to t_c^+} \dot{x}_2(t)$, which is equal to

$$\lim_{t \to t_c^+} \left\{ \frac{v^2 - x_2(t)^2}{x_1} - \underbrace{\hat{f} f(t)}_{-1} u(t) \sqrt{v^2 - x_2^2} \right\} \tag{67}$$

that is, because of $t \to t_c^+ \Rightarrow x_2 \to v^-$, we can rewrite it as

$$\lim_{x_2 \to v^-} \sqrt{v^2 - x^2} \left\{ \frac{\sqrt{v^2 - x_2(t)^2}}{x_1} + u(t) \right\} \tag{68}$$

then using reasoning (62)–(64), we can conclude that $\dot{x}_2(t_c^+) > 0$, which is impossible because $x_2(t_c) = v$ and $-v \leqslant x_2(t) \leqslant v$. Therefore, by contradiction, $\hat{f} = f(t_c^+)$, in which case $\dot{x}_2(t_c^+) < 0$.

The similar analysis for $\hat{f} = f(t_c^-)$, $\hat{f} = f(t_c^+)$, the limit $\lim_{t \to t_c^+} \dot{x}_2(t)$ and $t \to t_c^+ \Rightarrow x_2 \to -v^+$ results in

$$\lim_{t \to t_c^+} \dot{x}_2(t) = \lim_{\varepsilon \to 0^+} \sqrt{\varepsilon} \sqrt{2v} \left\{ \frac{\sqrt{2v}\sqrt{\varepsilon}}{x_1} - \omega_{max} \right\} \tag{69}$$

which means that $\lim_{t \to t_c^+} \dot{x}_2(t) \to 0^-$, that is, that $\dot{x}_2(t_c^+) < 0$, which is impossible because $x_2(t_c) = -v$ and $-v \leqslant x_2(t) \leqslant v$. Therefore, by contradiction, $\hat{f} = f(t_c^+)$ and because of that, $\dot{x}_2(t_c^+) > 0$.

Part c: For the case when $x_1(t_c) = 0$, we can consider the time point t_c as the initial time point and use Lemma 2 to infer that after a small τ $x_1(\tau) > 0$, $|x_2(\tau)| < v$ and $f(\tau) = \hat{f}$. The same can be inferred from Lemma 2 for the initial conditions with $x_1(0) = 0$ or $x_1(0) > 0$ and $|x_2(0)| = v$.

In summary, the results of Lemma 5 provide that in the case $\hat{f} \neq f(t)$, the system trajectories reach a time point t_c where $|x_2(t_c)| = v$ or $x_1(t_c) = 0$. In Part *a* of this proof, we showed that after the point $x_1(t_c) > 0$, $|x_2(t_c)| = v$, that is, for $t > t_c$, $\hat{f} = f(t)$. However, if $\hat{f} = f(t)$ and at a time point t_c, the system reaches a state with $|x_2(t_c)| = v$, then using the argument of Part *b*, we proved that $f(t)$ does not change, that is, we have that for $t > t_c$, $\hat{f} = f(t)$. In all cases has $\dot{x}_2$ pointing inside the trapping region. Finally, Part *c* uses arguments of Lemma 2 showing that for $x_1(t_c) = 0$ and the special initial conditions $x_1(0) = 0$, or $x_1(0) > 0$ and $|x_2(0)| = v$, the trajectory stays in the trapping region and $f(t) = \hat{f}$.

Therefore, under the assumption of the theorem, we conclude that after a sufficiently long time (including zero if $\hat{f} = f(0)$), the system trajectories are trapped in the region of the x_1-x_2 plane bounded by the segments $x_1 = 0$, $x_2 = v$, $x_1 = R_{max}$ and $x_2 = -v$ with $\hat{f} = f(t)$.

Lemma 6

If $\sqrt{d_{min} \frac{c_1(R_{max} - 2d_{min} - d)}{c_2}} > v$, then (*a*) $x_1(t) \geqslant R_{max} - 2d_{min}$ and $x_2(t) \geqslant 0 \Rightarrow u(t) = \omega_{max}$, which is the assumption A2 (5); and (*b*) under this condition, for any initial distance $x_1(0) \leqslant R_{max} - 2d_{min}$ and the control (30)–(32) results in $x_1(t) \leqslant R_{max}$, which is the corollary A2' (6).

DOI: 10.1002/rnc

Proof
To prove (a), we need to show that for all $x_1 \in [R_{max} - 2d_{min}, R_{max}]$ and $x_2 \in [0, v]$

$$u_c(x_1, x_2) = \left(\frac{c_1(x_1 - d)}{c_2\sqrt{v^2 - x_2^2}} + \frac{\sqrt{v^2 - x_2^2}}{x}_1 + \frac{c_3 x_2}{\sqrt{v^2 - x_2^2}} \right) > \omega_{max} \tag{70}$$

We first substitute all denominators with their maximal values to obtain

$$u_c(x_1, x_2) > \frac{c_1(x_1 - d)}{c_2 v} + \sqrt{v^2 - x_2^2} R_{max} + \frac{c_3 x_2}{v} \tag{71}$$

after the substitution of $\sqrt{v^2 - x^2}$ with v and x_1 with R_{max}. Then we substitute all numerators with their minimal values to obtain

$$u_c(x_1, x_2) > \frac{c_1(R_{max} - 2d_{min} - d)}{c_2 v} \tag{72}$$

after the substitution of $\sqrt{v^2 - x_2^2}$ with 0, x_2 with 0 and x_1 with $R_{max} - 2d_{min}$. If the right side of the last inequality is greater than $\omega_{max} = v/d_{min}$, then $u_c > \omega_{max}$, that is, $u = \omega_{max}$. This condition can be written as

$$\frac{c_1(R_{max} - 2d_{min} - d)}{c_2 v} > \frac{v}{d_{min}} \tag{73}$$

which is

$$\sqrt{d_{min} \frac{c_1(R_{max} - 2d_{min} - d)}{c_2}} > v \tag{74}$$

To prove (b), we will use Figure 6. Based on (a), once r reaches the distance $S = R_{max} - 2d_{min}$ and is moving away from the center O, $\dot{r} = x_2 > 0$, the vehicle spins with the maximal turning rate ω_{max}, which corresponds to the vehicle crossing the circle R_{max} with an angle between 0 and π to the tangent at the crossing point A. For the vehicles at A and A', this angle is smaller than $\pi/2$ and for the vehicle A'', the angle is greater that $\pi/2$. Without losing the generality of our analysis, we will discuss the vehicle at A.

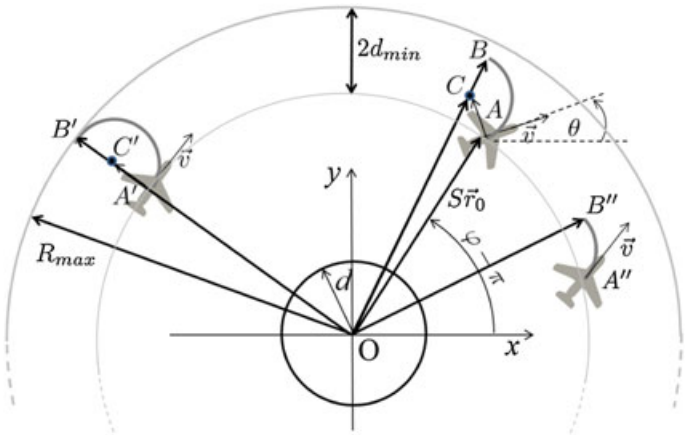

Figure 6. The Dubins vehicle model variable definitions. [Colour figure can be viewed at wileyonlinelibrary.com]

DOI: 10.1002/rnc

After the crossing point, the vehicle moves along the arc with the radius d_{min}. The vector from the position A to the center of the vehicle's orbit C has the length d_{min}, and it is orthogonal to the vehicle's velocity, which can be written as

$$\overrightarrow{AC} = d_{min}\,\vec{k} \times \vec{v}/v = d_{min}\left(-\sin\theta_A\vec{i} + \cos\theta_A\vec{j}\right) \tag{75}$$

and substituted in the vector expression for $\overrightarrow{OC}$, which is

$$\overrightarrow{OC} = \overrightarrow{OA} + \overrightarrow{AC} = (S\vec{r}_A + d_{min}\left(-\sin\theta_A\vec{i} + \cos\theta_A\vec{j}\right) \tag{76}$$

$$= (S\cos(\varphi_A - \pi) - d_{min}\sin\theta_A)\vec{i} + S(\sin(\varphi_A - \pi) + d_{min}\cos\theta_A)\vec{j} \tag{77}$$

where the vector $\overrightarrow{OA}$ is expressed by its magnitude S and the unit intensity vector $\vec{r}_A$. Now the distance $|\overrightarrow{BC}|$ can be expressed as

$$|\overrightarrow{BC}| = |\overrightarrow{OC}| + d_{min} = \sqrt{S^2 + d_{min}^2 - 2Sd_{min}\sin(\varphi_A - \theta_A)} + d_{min} \tag{78}$$

which yields its maximal value $\sup_{\varphi,\theta\in[0,2\pi)}|\overrightarrow{BC}| = S + d_{min} + d_{min} = R_{max}$ over all possible angles at which the vehicle can cross the circle $R_{max} - 2d_{min}$. Therefore, independently of $f(t) \neq \hat{f}$ or $f(t) = \hat{f}$, the maximal distance that can be reached by the vehicle is R_{max}.

At the crossing point A, the vehicle either has $f(t) \neq \hat{f}$ in which case it goes through the point with $x_2 = v$ after which $f(t) = \hat{f}$ (Lemma 3), or it starts from the point at which $f(t) = \hat{f}$ (for example, vehicle A''). In either case, once the vehicle reaches the point B with $x_2(t_B) = 0$, we have $f(t_B) = \hat{f}$. Now from the expression, we can conclude that $\dot{x_2} < 0$ for $x_1 = R_{max}$ and also for all $x_1 > d$, which means that after the point $x_2(t_B) = 0$, the vehicle never crosses the distance $|OB|$. This also applies to the specific case of the arc with the maximal distance $|OB| = R_{max}$, and with this, we conclude our proof. □

Theorem 1
Under conditions (C1)–(C3) ((33)–(36)), systems (16) and (17) under controls (30)–(32) have the stable fixed point $(d, 0)$, and all system trajectories converge to it.

Proof
In the case of controls (30)–(32), if (C1) is satisfied, then Lemma 3 through Lemma 5 are valid. Based on Lemma 5, we already know that the boundary A, B, C, D (Figure 3) forms the trapping region for the system trajectories and that $\hat{f} = f(t)$ holds after a sufficiently long time, including zero time if $\hat{f} = f(0)$.

The proof of the theorem is divided in three parts. The conclusion of Part1 is that the system can have a limit cycle within the trapping region to which trajectories can converge. Part 2 analyzes the vector field of the feedback controlled system for $x_2 = 0$. In Part 3, we show that the limit cycle cannot exist, which means that the trajectories can stay in the trapping region only by converging to the fixed point $(d, 0)$.

Part 1: Under controlS (30)–(32), the point d at $(d, 0)$ is the single fixed point of (16) and (17), and at this point, the control is not saturated ($0 < u = u_c < v/d < \omega_{max}$). Therefore, at that point, the closed loop system is described by linear systems (23) and (24). The stability of the point $(d, 0)$ depends on its eigenvalues λ_1 and λ_2 (34), which are both real and negative, $\lambda_2 < \lambda_1 < 0$ if $c_3 > 2\sqrt{c_1/c_2}$. Consequently, under this condition ($C2$), the point $(d, 0)$ is locally stable.

The two eigenvalues define two eigenvectors $[1\ \lambda_1]^T$ and $[1\ \lambda_2]^T$ that can be used to define four line segments going from the point $(d, 0)$ to the boundary A, B, C, D. The segments are defined as

$$\overline{da} : x_2 = \lambda_1(x_1 - d), x_2 \in [0, v] \tag{79}$$

DOI: 10.1002/rnc

$$\overline{db} : x_2 = \lambda_2(x_1 - d), x_2 \in [-v, 0] \tag{80}$$

$$\overline{dc} : x_2 = \lambda_1(x_1 - d), x_2 \in [-v, 0] \tag{81}$$

$$\overline{de} : x_2 = \lambda_2(x_1 - d), x_2 \in [0, v] \tag{82}$$

If we consider the combination x_1, x_2 along these four segments, we will find that along $\overline{da}$ and $\overline{de}$, the control variable ω saturates on the interval $(0, d)$ as $x_1 \to 0$. We can also find that because $\lambda_2 < \lambda_1 < 0$, along the line $\overline{db}$, the control saturates for a smaller x_1 as $x_2 \to -v$ than on the line $\overline{dc}$. Therefore, the focus of our analysis is on the line $\overline{dc}$.

If the control is not saturated on the line $\overline{dc}$ on the interval up to a value of $r_{max} > d$, then the closed loop system is described by linear systems (23) and (24) not only at point $(d, 0)$ but also on the whole segment where $d < x_1 < r_{max}$. The line $\overline{dc}$ corresponds to the eigenvector of the linear system, therefore, if the system state reaches the line and $x_1 < r_{max}$, the state will converge to the point $(d, 0)$ along it. Now let us write the condition providing that $u_c < \omega_{max} = v/d_{min}$, which yields $C3$, and set $R_{max} = r_{max}$, which defines the BC boundary of the trapping region.

Inside the boundary A, B, C, D, there are no other fixed points; therefore, no other point to which the system trajectories can converge. However, according to the Poincaré–Bendixson theorem [31], this does not exclude the possibility of system trajectories converging to the limit cycle inside the boundary. Inside the boundary A, B, C, D, we can have a cycle that does not go through $x_1 = 0$ and a cycle that goes through $x_1 = 0$, which is the conclusion from this part of the proof.

Part 2: Before we continue with the rest of the proof, let us analyze the vector field of the system for $x_2 = 0$. Because $\dot{x}_1 = x_2$, it means that along the line x_2, the vector field is orthogonal to the line and we just need to find its direction from the sign of $\dot{x}_2$.

(a) If the control is not saturated, that is, $-\omega_{max} < u_c < \omega_{max}$, then we know from (24) that for $x_2 = 0$

$$\dot{x}_2 = -\frac{c_1(x_1 - d)}{c_2} \tag{83}$$

and can conclude that $\dot{x}_2 > 0$ for $x_1 > d$ and $\dot{x}_2 < 0$ for $0 < x_1 < d$.

(b) On the interval $x_1 > d$, if the control is saturated, then from (32) for $x_2 = 0$, it must be $u_c > \omega_{max}$ and when $u = \omega_{max}$ is substituted in (17), we obtain

$$\dot{x}_2 = \frac{v^2}{x_1} - \omega_{max} v = \frac{v^2}{x_1} - \frac{v^2}{d_{min}} \tag{84}$$

which means that $\dot{x}_2 < 0$ for all $x_1 > d$.

(c) On the interval $0 < x_1 < d$, if the control is saturated with $u_c > \omega_{max}$, then for $x_2 = 0$ in (32), we obtain the condition

$$\frac{c_1(x_1 - d)}{c_2} > -\frac{v^2}{x_1} + \frac{v^2}{d_{min}} \tag{85}$$

Based on the signs of the left and the right sides of the inequality, this can be satisfied only if $0 < x_1 < d_{min}$, which means that for $d_{min} \leqslant x_1 < d$, the control cannot be saturated.

After the substitution of $u = \omega_{max}$ in (17), we obtain (87) and conclude that $\dot{x}_2 > 0$ for all $0 < x_1 < d_{min}$. For the interval $d_{min} < x_1 < d$ where the control is not saturated from (a) (expression (83)) of this part of the proof, we know that $\dot{x}_2 > 0$. With this, we can conclude that $\dot{x}_2 > 0$ for all $0 < x_1 < d$.

(d) On the interval $0 < x_1 < d$, if the control is saturated with $u_c < -\omega_{max}$, then for $x_2 = 0$ in (32), we obtain the condition

$$\frac{c_1(x_1 - d)}{c_2} > -\frac{v^2}{x_1} - \frac{v^2}{d_{min}} \tag{86}$$

DOI: 10.1002/rnc

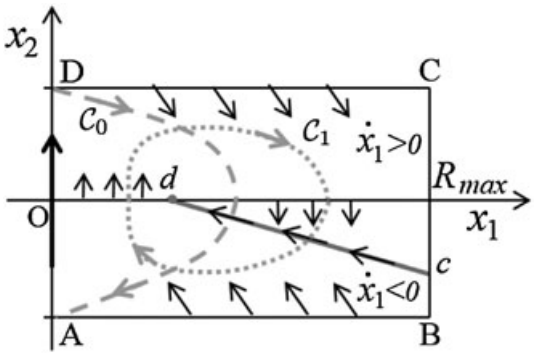

Figure 7. Hypothetical limit cycles $\mathcal{C}_0$ and $\mathcal{C}_1$.

that can be satisfied on the whole interval $0 < x_1 < d$. In this case, $u = -\omega_{max}$ and when substituted in (17), we obtain

$$\dot{x}_2 = \frac{v^2}{x_1} + \omega_{max} v = \frac{v^2}{x_1} + \frac{v^2}{d_{min}} \tag{87}$$

which means that $\dot{x}_2 > 0$ for all $0 < x_1 < d$.

From (a) and (b), we conclude that $\dot{x}_2 < 0$ for $x_1 > d$, and from (c) and (d), we conclude that $\dot{x}_2 > 0$ for $0 < x_1 < d_{min}$. The vector field arrows resulting from this analysis for $x_2 = 0$ are depicted in Figure 7 as orthogonal arrows to the axis x_1.

Part 3: If the cycle does not go through $x_1 = 0$, then we should note that the control is continuous (continuous vector field) within the boundary in which the cycle exists. By index theory [32], the cycle has to encircle the point d, and this type of hypothetical cycle $\mathcal{C}_1$ is depicted with the gray dotted line in Figure 7. For details on the application of index theory to continuous vector fields, see [33, 34], and, specifically, [35] (property 3, page 148). Therefore, the cycle has to cross the line $\overline{dc}$ from the condition $C3$. However, on the line up to R_{max}, which defines the right bound of the trapping region, the control is not saturated, and on that line, the system trajectories satisfy (23) and (24). Consequently, if the cycle trajectory crosses the line, it will stay on the line, and because of the negative eigenvalue, it will converge along the line toward the fixed point $(d, 0)$. Therefore, the limit cycle $\mathcal{C}_\infty$ with $x_1(t) \neq 0$ cannot exist.

If the cycle goes through $x_1 = 0$, then it goes through the points A $(x_1 = 0, x_2 = -v)$ and $D[(x_1 = 0, x_2 = v)$ of the trapping region. Once the cycle trajectory is at D, it has to return to the point A as presented in Figure 7 depicting this type of hypothetical cycle $\mathcal{C}_0$ with the gray dashed line. However, from Part 2 of this proof, we know that $\dot{x}_2 > 0$ for $0 < x_1 < d$, which means that the only path for the cycle trajectory from the point $D](x_1 = 0, x_2 = v)$ to the point $A(x_1 = 0, x_2 = -v)$ is to cross the axis $x_2 = 0$ and the line $\overline{dc}$. From it, we can also conclude that the cycle $\mathcal{C}_0$, which includes the point $x_1 = 0$, cannot exist.

Because the possibility of system trajectories converging to a limit cycle is excluded, we can conclude that all trajectories converge to the single stable fixed point $(d, 0)$.

□

6. PARAMETER SELECTION

The results of the previous sections define the constraints on the c_1, c_2, and c_3 selection, so that the vehicle converges toward the point $(d, 0)$ and circumnavigates in the desired direction, which depends on the choice of $\hat{f}$. The constraints do not define the selection of particular parameter values. However, based on constraints (C1)–(C3) ((33)–(36)) and defined controls (31) and (32), the selection of parameters can be reduced to choosing the ratio c_1/c_2 and c_3.

Among many approaches to parameter selection, we may choose to linearize the model around the point $(d, 0)$ and select parameters based on the linear control design, for example, using the LQR controller [36].

DOI: 10.1002/rnc

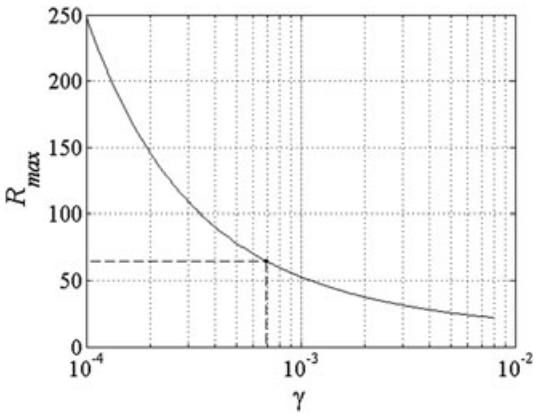

Figure 8. Combinations of the controller's maximal range R_{max} and parameter γ values.

If we introduce the variables $\tilde{x}_1 = x_1 - d$ and $\tilde{x}_2 = x_2$ and $\tilde{u} = u - \frac{v}{d}$, then around the point $(d, 0)$ and $\hat{f} = f(t)$, our systems (16) and (17) can be approximated as the following linear system:

$$\begin{bmatrix} \dot{\tilde{x}}_1 \\ \dot{\tilde{x}}_2 \end{bmatrix} = \underbrace{\begin{bmatrix} 0 & 1 \\ -\frac{v^2}{d^2} & 0 \end{bmatrix}}_{A} \begin{bmatrix} \tilde{x}_1 \\ \tilde{x}_2 \end{bmatrix} + \underbrace{\begin{bmatrix} 0 \\ -v \end{bmatrix}}_{B} \tilde{u} \tag{88}$$

As an example of using the linear design for parameter selection, we choose to use a linear quadratic criterion

$$J = \int_0^\infty \left(\gamma \tilde{x}_1^2 + \tilde{x}_2^2 + \tilde{u}^2\right) dt = \int_0^\infty \left([\tilde{x}_1 \ \tilde{x}_2] \underbrace{\begin{bmatrix} \gamma & 0 \\ 0 & 1 \end{bmatrix}}_{Q} \begin{bmatrix} \tilde{x}_1 \\ \tilde{x}_2 \end{bmatrix} + \tilde{u}^2 \right) dt \tag{89}$$

For the given linear system and value of γ, the LQR design defines the control as $\tilde{u} = k_1\tilde{x}_1 + k_2\tilde{x}_2$. Based on the definition of $\tilde{x}_1$ and $\tilde{x}_2$, it is clear from (32) and the feedback linearization nature of that control that two feedback gains k_1 and k_2 can be associated with the ratio c_1/c_2 and c_3, respectively.

For $\gamma > 0$, the matrix Q is positive definite, and for $\gamma > 0$, the matrices A and B form a controllable pair, providing that the LQR controller can be computed for any $\gamma > 0$ (page 771, [36]). We use $0 < \gamma < 1$, which decreases the weight on the $x_1 - d$ term in our control, with the idea that it helps satisfy the conditions derived in the previous section, specifically if we would like to consider larger values of x_1 in our control design.

In our examples, we use the following vehicle parameters, $v = 1$, $d_{min} = 4.5$ and the desired radius $d = 10$. We compute the LQR controller based on (88) and (89) for various values of γ and check conditions (C1) to (C3). This gives the range of γ and corresponding R_{max} values. These combinations are plotted in Figure 8. Once we specify R_{max}, we can read γ from the diagram and use it to compute k_1 and k_2. At the points where the diagram is not plotted, there are no γ values providing that (C1) to (C3) are satisfied.

As the consequence of the parameter values $c_1 = 0.8$, $c_2 = 11$, and $c_3 = 4$ corresponding to $k_1 = c_1/c_2 = 0.07273$ and $k_2 = c_3$, which are used in our previous work and satisfy (C1) to (C3), we use $R_{max} = 64.56$. For these parameters, the eigenvalues are $\lambda_1 = -0.0183$ and $\lambda_2 = -3.9817$. The parameter values are not selected by any optimization; therefore, they can serve us well to see if there are any benefits of using the LQR designed feedback gains k_1^{LQR} and k_2^{LQR}. From the diagram in Figure 8, we can read that for $R_{max} = 64.56$, $\gamma = 6.92 \cdot 10^{-4}$, which results into the feedback gains $k_1^{LQR} = 0.0181$ and $k_2^{LQR} = 1.0180$ and the eigenvalues $\lambda_1^{LQR} = -0.0181$ and $\lambda_2^{LQR} = -0.9998$.

DOI: 10.1002/rnc

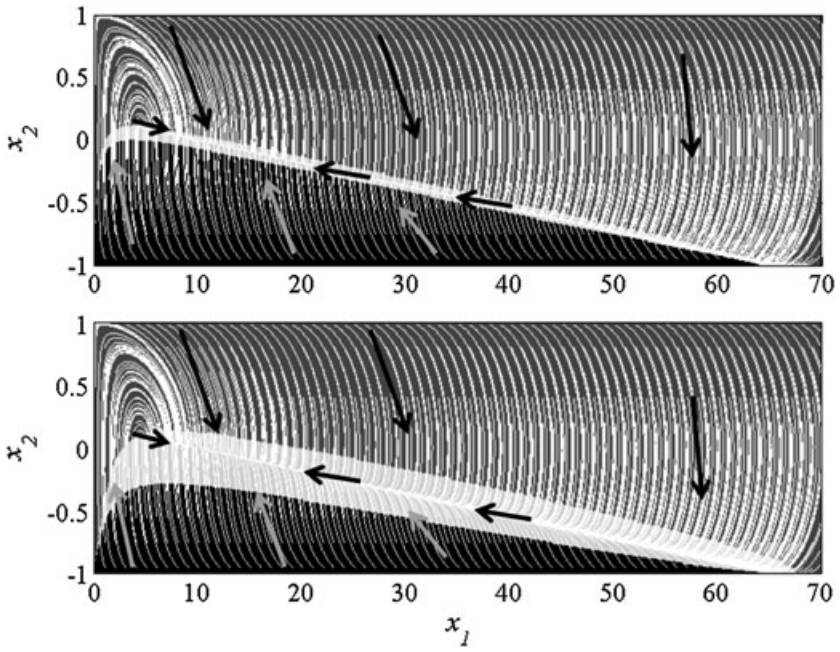

Figure 9. Phase portraits for non-optimal (top panel) and optimal (bottom panel) feedback gains.

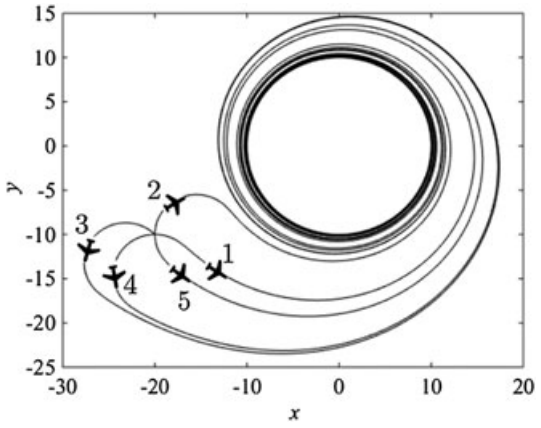

Figure 10. Simulation results for $\hat{f} = 1$, $x(0) = -20$, $y(0) = -10$ and various initial heading angles.

The effects of nonoptimal $k_1 = c1/c_2$, $k_2 = c_3$ and optimal $k_1 = k_1^{LQR}$, $k_2 = k_2^{LQR}$ feedback gains can be compared by 2D phase portraits within the trajectory trapping region pointed by Lemma 5 in which $f(t) = \hat{f}$. The upper panel of Figure 9 shows the phase portrait for nonoptimal feedback gains, while the lower panel shows the phase portrait for optimal feedback ones. The trajectory directions are depicted with arrows and the region with control $u = u_{max}$ is given in medium gray, the region with $u = -u_{max}$ in dark and the non-saturating region, in which $-u_{max} < u < u_{max}$, in light gray. From the figure, it can be seen that the LQR feedback gains result in a controller with a larger non-saturating region. When we compare the eigenvalues, we see that $\lambda_1 < \lambda_1^{LQR} < 0$ and $\lambda_2 < \lambda_2^{LQR} < 0$, that is, $|\lambda_1| > |\lambda_1^{LQR}|$ and $|\lambda_2| > |\lambda_2^{LQR}|$. The most important eigenvalues to compare are λ_1 and λ_1^{LQR} because they define the convergence rate along the long segment $\overline{dc}$ (Figure 3) and the slope of it, that is, the maximal range of the controller R_{max}. Because the range R_{max} is the same in these two cases, we find that $|\lambda_1^{LQR}|$ is insignificantly different from $|\lambda_1|$. Therefore, we can conclude that with the optimal feedback gains, the overall performance of the controller is slightly sacrificed, while the non-saturating region is enlarged.

DOI: 10.1002/rnc

7. EXAMPLE

To illustrate the work of the controller, we use the same parameters as in the previous section, $v = 1$, $d = 10$, $d_{min} = 4.5$. We first show the vehicle trajectories for the control feedback gains, $k_1 = k_1^{LQR}$ and $k_2 = k_2^{LQR}$, which are computed in the previous section. Then, we point to differences in the simulation results when $k_1 = c_1/c_2$ and $k_2 = c_3$.

Our simulation results are based on the following simulation algorithm, where k denotes the discrete time step index and ΔT is the sample time:

Loop:

1. $k = k + 1$
2. $x_1 = r(k) = \sqrt{x(k)^2 + y(k)^2}$
3. Compute the rate of change estimation: $\hat{x}_2 = \frac{1}{\Delta T}(r(k) - r(k-1))$
4. Compute the control $u(k)$:

$$u_c = \begin{cases} \frac{1}{v^2 - \hat{x}_2^2}\left(\frac{c_1(x_1 - d)}{c_2} + \frac{v^2 - \hat{x}_2^2}{x_1} + c_3\hat{x}_2\right), & x_1 \neq 0 \\ \omega_{max}, & \hat{x}_1 = 0 \end{cases}$$

$$u(k) = \begin{cases} \omega_{max}, u_c > \omega_{max} \\ -\omega_{max}, u_c < -\omega_{max} \\ u_c, \text{otherwise} \end{cases}$$

5. Compute $x(k+1)$, $y(k+1)$ and $\theta(k+1)$ by solving (1)–(3) on the interval $[k, k + 1\Delta T]$ with the turning rate $\omega = \hat{f}u(k)$ and initial condition $x(k)$, $y(k)$, $\theta(k)$.

Note that in the simulation algorithm, we intentionally do not use a value of $x_2(k)$ that can be computed based on $x(k)$, $y(k)$ and $\theta(k)$, but $\hat{x}_2$, which is based only on the range x_1 that can be measured. Step 5 of the loop is the simulation substitute for a real vehicle controlled with the sample time ΔT. In our case, $\Delta T = 0.1s$.

For the control parameters $k_1 = k_1^{LQR} = 0.0181$ and $k_2 = k_2^{LQR} = 1.0180$ in Figure 10, we show the results of five trajectory examples starting with the same initial position $x(0) = -20$, $y(0) = -10$ and initial heading angles $\theta(0) = 0, \frac{\pi}{2}, \frac{3\pi}{4}, \pi, -\frac{\pi}{2}$ corresponding to the trajectories labeled with 1 to 5, respectively, in Figure 10. These trajectories are almost identical to those obtained for $k_1 = c_1/c_2$ and $k_2 = c_3$. This is because almost all trajectories that start at a distance greater than the radius $d = 10$ in the $x_1 - x_2$ space (Figure 9, bottom panel) converge to the line segment $\overline{dc}$ (Figure 3) defined by the eigenvalue λ_1^{LQR}, which is practically the same as λ_1. The corresponding control for each initial heading angle is depicted in Figure 11. We see that for

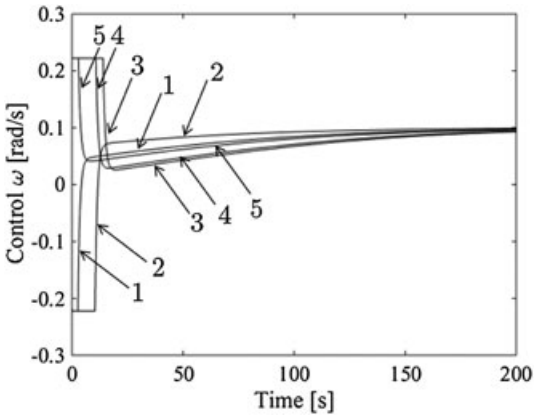

Figure 11. Control from the simulation results depicted in Figure 10.

DOI: 10.1002/rnc

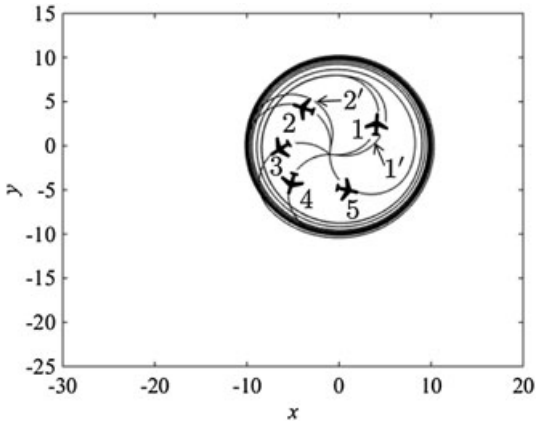

Figure 12. Simulation results for $\hat{f} = 1$, $x(0) = -1$, $y(0) = -1$ and various initial heading angles.

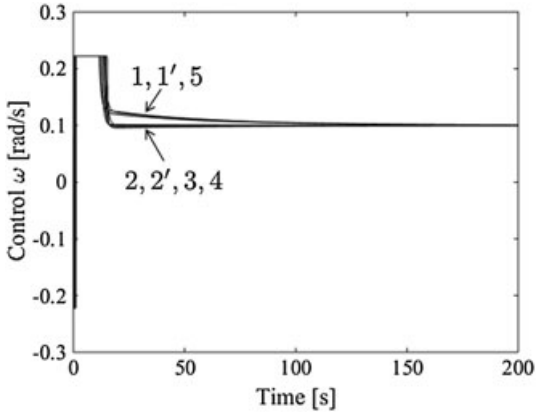

Figure 13. Control from the simulation results depicted in Figure 12.

all cases after $20s$, the control is not saturated and converges to the value 0.1, which maintains the vehicle on the circular trajectory of the radius $d = 10$.

The difference between trajectories under the two sets of controller's parameters is more visible if we consider trajectories that start within the range d. Figure 12 shows the simulation results for the initial position $x(0) = -1$, $y(0) = -1$. All trajectories are simulated for $\hat{f} = 1$, $v = 1$, $d = 10$, $d_{min} = 4.5$. The trajectories resulting from the feedback gains $k_1 = k_1^{LQR} = 0.0181$ and $k_2 = k_2^{LQR} = 1.0180$ are labeled by the aircraft symbols, while those resulting from the feedback gains $k_1 = c_1/c_2 = 0.07273$ and $k_2 = c_3 = 4$ are unlabeled. The trajectories for the two sets of feedback gains are almost identical for the initial heading angles $\theta = 3\pi/4$, $\theta = \pi$ and $\theta = -\pi/2$ (Figure 12, labels 3, 4, and 5, respectively), while for the initial angles $\theta = 0$, $\theta = \pi/2$ (Figure 12, labels 1 and 2), they are different. The trajectory shapes are the result of the phase portrait complexity to the left of $x_1 = d = 10$ (Figure 9). It turns out that in this case, the trajectories for the nonoptimal feedback gains $k_1 = c_1/c_2$ and $k_2 = c_3$ converge faster to the desired radius if the initial heading angles are $\theta = 0$ and $\theta = \pi/2$. The corresponding control for each initial heading angle is depicted in Figure 13. We see that for all that, the contol is initially saturated for a short period and then converges to the value 0.1, which maintains the vehicle on the circular trajectory of the radius $d = 10$.

These simulation results suggest that while the LQR design-based parameter selection is useful for establishing the relation between the control design parameters and the range of the controller, there are other ways to define an optimal selection of control parameters. Independently of an exact procedure for the selection of the parameters, they need to be validated against the constraints established in this paper.

DOI: 10.1002/rnc

8. CONCLUSIONS

In this paper, the Dubins vehicle circumnavigation controller based on the analysis of the state space dynamics resulting from the state transformation has been derived. The model state variables are range, range rate, and a discrete variable, which relates to the direction of the circumnavigation around the center of the vehicle's trajectory. Because the discrete value can take only two values, it can be concluded that the discrete variable value can be guessed and that the controller's convergence to the circular path is warrantied even if the guess is incorrect. Therefore, the proposed feedback controller is based on range and range rate measurements and does not require any information about the direction to the center of the trajectory, or the direction of the motion. However, the range in which the controller can work is bounded, and the controller's parameters have to be selected based on the trade-off between the working range and the rate of the convergence of the vehicle's trajectory to the circular path. The trade-off has been illustrated by the controller's parameters resulting from the LQR design method, but alternative controller parameter selection methods are allowed as far as parameters satisfy the conditions presented in this paper.

Although rigorously speaking the controller needs range and range rate measurements, the latter can be estimated from the first, and the overall controller can be considered as a nonlinear proportional-differential controller based on range measurements. While the controller is derived for range measurements, any other type of measurements that is proportional to range measurements can be used, for example, signal intensity. In this case, the signal source would be placed in the center of the desired circular trajectory, and the navigation of the vehicle would be based on the received signal strength. Provided that there are multiple signal sources around which the vehicle can circumnavigate in a sequence, the presented controller can be used to navigate the vehicle without the GPS.

ACKNOWLEDGEMENTS

We are thankful to the anonymous reviewers for their comments that helped us improve the manuscript and the journal's editor Professor Jeffrey Cook, University of Michigan, for his excellent guidance through the review process. We are also thankful to Prof. Steven H. Strogatz, Cornell University, who helped us clarify the application of index theory to continuous vector fields and pointed us to the important references.

REFERENCES

1. Beard RW, McLain TW. *Small Unmanned Aircraft: Theory and Practice*. Princeton University Press: Princeton, NJ, 2012.
2. Warwick G. *Independent tests confirm GPS jamming by LightSquared. Aviation Week*, June 2011. [Online]. Available: http://aviationweek.com/awin/independent-tests-confirm-gps-jamming-lightsquared-0 (retrieved on December 14, 2014).
3. Shepard D, Bhatti J, Humphreys T. *Drone hack: Spoofing attack demonstration on a civilian unmanned aerial vehicle. GPS World*, August 2012. [Online]. Available: http://www.gpsworld.com/drone-hack/ (retrieved on December 14, 2014).
4. Sahinoglu Z, Gezici S. Ranging in the IEEE 802.15.4a standard. *Proceedings of IEEE Annual Wireless and Microwave Technology Conference*, Clearwater Beach, FL, 2006; 1–5.
5. Dai R, Cochran JE. Path planning and state estimation for unmanned aerial vehicles in hostile environments. *Journal of Guidance, Control, and Dynamics* 2010; **33**(2):595–601.
6. McGee TG, Hedrick JK. Optimal path planning with a kinematic airplane model. *Journal of Guidance, Control, and Dynamics* 2007; **30**(2):629–633.
7. Anderson RP, Bakolas E, Milutinović D, Tsiotras P. Optimal feedback guidance of a small aerial vehicle in a stochastic wind. *Journal of Guidance, Control, and Dynamics* 2013; **36**(4):975–985.
8. Anderson RP, Milutinović D. On the construction of minimum-time tours for a dubins vehicle in the presence of uncertainties. *Journal of Dynamic Systems, Measurement, and Control* 2014; **137**(3):031007 (8 pages).
9. Rubio JC, Vagners J, Rysdyk R. Adaptive path planning for autonomous UAV oceanic search missions. *Proceedings of AIAA 1st Intelligent Systems Technical Conference*, paper ID: AIAA, Chicago, IL, 2004; 2004–6228.
10. Obermeyer KJ. Path planning for a UAV performing reconnaissance of static ground targets in Terrain. *Proceedings of AIAA Guidance, Navigation, and Control Conference*, paper ID: AIAA, Chicago, IL, 2009; 2009–5888.
11. Qu Z, Xi X, Girard A. Cooperative UAV trajectory planning with multiple dynamic targets. *Proceedings of AIAA Guidance, Navigation, and Control Conference*, paper ID: AIAA, Toronto, Canada, 2010; 2010–8437.

DOI: 10.1002/rnc

12. Tang Z, Ozguner U. Motion planning for multitarget surveillance with mobile sensor agents. *IEEE Transactions on Robotics* 2005; **21**(5):898–908.
13. Deghat M, Shames I, Anderson BDO, Yu C. Localization and circumnavigation of a slowly moving target using bearing measurements. *IEEE Transactions on Automatic Control* 2014; **59**(8):2182–2188.
14. Shames I, Dasgupta S, Fidan B, Anderson BDO. Circumnavigation using distance measurements under slow drift. *IEEE Transactions on Automatic Control* 2012; **57**(4):889–903.
15. Summers TH, Akella MR, Mears M. Coordinated standoff tracking of moving targets: control laws and information architectures. *Journal Of Guidance, Control, and Dynamics* 2009; **32**(1):55–69.
16. Nelson DR, Barber DB, McLain TW, Beard 0. Vector field path following for miniature air vehicles". *IEEE Transactions on Robotics* 2007; **23**(3):519–529.
17. Park S, Deyst J, How JP. Performance and Lyapunov stability of a nonlinear path-following guidance method. *Journal of Guidance, Control, and Dynamics* 2007; **30**(6):1718–1728.
18. Lawrence DA, Frew EW, Pisano WJ. Lyapunov vector fields for autonomous unmanned aircraft flight control. *Journal of Guidance, Control, and Dynamics* 2008; **31**(5):1220–1229.
19. Anderson R, Milutinović D. A stochastic approach to dubins vehicle tracking problems. *IEEE Transactions on Automatic Control* 2014; **59**(10):2801–2806.
20. Cao Y, Muse J, Casbeer D, Kingston D. Circumnavigation of an unknown target using UAVs with range and range rate measurements. *Proceedings of the 52nd IEEE Conference on Decision and Control (CDC)*, Florence, Italy, 2013; 3617–3622.
21. Hashemi AR, Cao Y, Yin G, Casbeer D. UAV circumnavigation using noisy range-based measurements without gps information. *ASME Journal of Dynamic Systems Measurement and Control* 2014; **137**(3):031003-031003-10.
22. Dubins LE. On curves of minimal length with a constraint on average curvature, and with prescribed initial and terminal positions and tangents. *American Journal of Mathematics* 1957; **79**(3):497–516.
23. Ren W, Beard R. Trajectory tracking for unmanned air vehicles with velocity and heading rate constraints. *IEEE Transactions on Control Systems Technology* 2004; **12**(5):706–716.
24. Teimoori H, Savkin AV. Equiangular navigation and guidance of a wheeled mobile robot based on range-only measurements. *Robotics and Autonomous Systems* 2010; **58**(2):203–215.
25. Matveev AS, Teimoori H, Savkin AV. The problem of target following based on range-only measurements for car-like robots. *Joint 48th IEEE Conference on Decision and Control and 28th Chinese Control Conference*, Shanghai, P.R. China, 2009; 16–18.
26. Samson C. Time-varying feedback stabilization of car-like wheeled mobile robots. *The International Journal of Robotics Research* 1993; **12**(1):55–64.
27. Aicardi M, Casalino G, Bicchi A, Balestrino A. Closed loop steering of unicycle like vehicles via Lyapunov techniques. *IEEE Robotics & Automation Magazine* 1995; **2**(1):27–35.
28. Slotine J-JE, Li W. *Applied Nonlinear Control. Chapter 6*. Prentice Hall: Englewood Cliffs, NJ, 1991.
29. Milutinović D, Casbeer D, Cao Y, Kingston D. Coordinate frame free Dubins vehicle circumnavigation. *Proceedings of American Control Conference (ACC)*, Portland, OR, 2014; 891–896.
30. Slotine J-JE, Li W. *Applied Nonlinear Control. Chapter 3*. Prentice Hall: Englewood Cliffs, NJ, 1991.
31. Strogatz SH. *Nonlinear Dynamics and Chaos. Chapter 7*. Westview Press: Boulder, CO, 2000.
32. Strogatz SH. *Nonlinear Dynamics and Chaos. Chapter 6*. Westview Press: Boulder, CO, 2000.
33. Henle M. *A Combinatorial Introduction to Topology*. Dover Publications: New York, 1979.
34. Andronov AA, Leontovich EA, Gordon II, Maier AG. *Qualitative Theory Of Second-Order Dynamic Systems*. John Wiley & Sons, Israel Program for Scientific Translations, 1973.
35. Zhi-fen Z, Ton-ren D, Wen-zao H, Zhen-xi D. *Qualitative theory of differential equations*, Translations of Mathematical Monographs, vol. 101. American Mathematical Society: Providence, RI, 2006.
36. Athans M, Falb PL. *Optimal Control. Chapter 9*. Dover Publications: New York, 2007.

DOI: 10.1002/rnc